Dynamic modeling of a solar ORC with compound parabolic collectors: annual production and comparison with steady-state simulation.

A. Baccioli*, M. Antonelli, U. Desideri
Department of Energy, Systems, Territory and Construction Engineering (D.E.S.T.eC.), University of Pisa, Pisa, Italy
**email: andrea.baccioli@for.unipi.it; Tel: +39 050-2217137; Fax: +39 050-2217160*

Abstract

In this paper the dynamic behavior of a small low-concentration solar plant with static Compound Parabolic Collectors (CPC) and an ORC power unit with rotary volumetric expander has been analyzed. The plant has been simulated in transient conditions for a year-long operation and for three different sites respectively located in northern, central and southern Italy, in order to evaluate the influence of the latitude on the production. Hourly discretized data for solar radiation and for ambient temperature have been used. The adoption of a sliding-velocity control strategy, has allowed to operate without any storage system with a solar multiple (S.M.) of 1, reducing the amplitude of the solar field and simplifying the control system. Different collectors tilt angles and concentration factors, as well as thermodynamic parameters of the cycle have been tested, to evaluate the optimal working conditions for each locality. Results highlighted that specific production increased with the concentration ratio, and with the decrease of latitude. The comparison with the steady-state analysis showed that this type of control strategy is suited for those configurations having a smaller number of collectors, since the thermal inertia of the solar field is not recovered at all during the plant shut-down phase.

1 Introduction

Nowadays, the interest towards solar energy has been raising more and more: the global installed solar thermal power reached 4287 MW in 2014 [1]. High temperature solar thermal power plants are suitable for large size because of the high cost of its component while Photovoltaic (PV) systems have been used for small scale solar plants. The coupling between static collector fields and ORC systems, can reduce the costs of solar thermal power plant and allows a downsizing of the system [2]. Static Compound Parabolic Collectors reach moderate concentration ratios without the need of tracking system, are easy for fabrication and have a lower cost compared to other concentrating collectors [3] for this reason this type of collectors results to be suitable for small scale applications. CPCs have been widely studied in the literature [4–8] [9–13] and many improvement have been evaluated to reduce thermal losses and increase the efficiency. CPCs collectors can be adapted to collect solar energy at low temperature and provide the heat necessary to make the ORC run in the characteristic field of applicability [14, 15].

Small scale ORCs allow the use of positive displacement expanders [16–21], characterized by low costs

[22–24], high simplicity, low rotational speed and a wide operating range. Due to the capacity of operating at different working conditions, several control strategies can be implemented when operating with volumetric expanders, increasing plant flexibility. This last characteristic is essential for small scale systems coupled with time variable energy sources. Many authors focused on the control strategies to improve the flexibility of small scale plants: Quoilin et al. [25] and Antonelli et al. [26] demonstrated that positive displacement expanders can be used both for sliding-pressure and for sliding-velocity control strategy: in the first control strategy, the plant power is controlled by varying the evaporating pressure of the cycle, keeping the expander speed at a constant value; in the second control strategy, the plant power is controlled by keeping the evaporating pressure at a constant set point value and varying the expander speed. A combination of both strategies can be found, which maximizes system efficiency [25], if system inertia is low.

Recently, many studies on power generation system were carried in transient conditions [27–30]. The dynamic modeling allowed a better understanding of the evolution of the various plant variables and in the recent years has become an important instrument to evaluate solar plant behavior. Dickes et al. in [31] simulated a 5 kWe solar ORC by using Modelica for 3 consecutive days with real meteorological data and found out that there are some benefits if the temperature at the outlet of the solar field and of the evaporator is kept constant. Vitte and Manenti et al. in [32,33] carried out numerical simulations to perform the start-up operations of the Archimede Concentrating Solar Plant in Sicily, using DYNSIM. Firstly, they carried out some simplified simulation to perform start-up and shut-down operations and identify the critical aspects and then with a more detailed simulation they optimized the control strategy of the plant. El Hefni in [34] tested the new library ThermoSysPro of Modelica dedicated to power production plants simulating firstly a linear parabolic trough solar power plant and then a solar hybrid combined power plant with linear Fresnel collectors. Rodat et al. in [35] analyzed the start-up, shut-down and response to perturbations of a Fresnel Solar Power Plant, calibrating and validating the model with data from an existing solar plant. Dynamic models can also be employed to improve prediction of the energy output of a solar system during one year of operation. Twomei et al. in [36], after calibrating the model of a scroll expander completed an annual dynamic simulation on a solar driven co-generated ORC with scroll expander, evaluating the total produced energy, with a solar field of 50m^2 of evacuated tubes. A monthly average value of irradiation was the input to build the solar irradiation during the 15th of each month, which was considered the sample day of the month. The numerical model provided the annual production and the effect of the storage volume on the delay of production. Mitterhofer et al. in [37] modeled a 3 kWe solar ORC with a rock-bed TES (Thermal Energy Storage) in Dymola: the thermal solar loop was modeled in dynamic conditions while the ORC module in steady-state. Zhou et al. in [38] designed and simulated in transient conditions a solar field to integrate a binary geothermal ORC with superheating: to reduce the complexity of the simulations and avoid control loops, only the solar field was simulated in dynamic conditions, and the steady-state results of the geothermal system were then summed to the transient results of the solar loop to obtain the annual production of the plant.

In a previous work, [39] a low concentration solar plant with ORC and rotary expander has been simulated in real condition for five consecutive days. The flexibility of the control strategy and of the expander, avoids the use of any storage system, reducing in this way the solar field extension: in fact, the maximum size of the collectors field was equal to the maximum thermal power of the ORC module and therefore the value of the solar multiple was 1. The thermal inertia of the Heat Transfer Fluid (HTF) inside the solar field provided a more gradual start-up and shut-down operation than that of a photovoltaic system, with a lower stress of the electric grid.

This work is the natural consequence of the previously published papers [39, 40]. In [40] a steady state model of a small size solar plant with CPCs collectors and Wankel expander was presented to determine the most effective type of evacuated pipe, while in [39] the feasibility of the sliding-velocity control strategy was tested in five consecutive days under different radiation conditions, to prevent the thermal storage. In this work, the low concentration solar plant with ORC cycle and rotary expander, reported in [39, 40], has been simulated during a year-long operation for different thermodynamic conditions and different solar field configurations, to evaluate the optimal thermodynamic operating parameters, the optimal tilt angle and the optimal concentration in three different areas in Northern, Central and Southern Italy. Static Compound Parabolic Collectors with evacuated pipes have been considered for the solar field. Differently from [36], where an average monthly irradiation was considered, in this work hourly discretized irradiation and temperature data were considered for each place and for the whole year. The effect of the absence of the thermal storage has been widely investigated, taking into account the transient behavior of both the solar field and of the ORC module: the scope of this paper is not to provide a precise information regarding the value of the plant production but to highlight the role of the various control variables and parameters on the plant transient behavior.

The comparison of the results with those of a steady-state model revealed that this type of control is more suited for those plant configurations that minimized the solar field inertia. To the authors knowledge this has been the first time that a solar system with a such type of control strategy has been simulated in transient conditions and with different thermodynamic and solar field parameters for a year-long of operation. Respect to other works in the literature, the implementation of all the main components of the system has provided useful information about the actual transient behavior of both the solar field and of the ORC module.

Nomenclature		**Subscripts**	
G	Radiation Intensity [W/m^2]	ad	Admission
I_{bn}	Direct Normal Radiation [W/m^2]	is	Isentropic
I_{do}	Diffuse Radiation [W/m^2]	w	Wall
i	Incidence Angle [deg]	hyd	Hydraulic
r	Ground reflectivity		
a	Azimuth [deg]		
a_c	Collector azimuth [deg]		
Nu	Nusselt Number		
Re	Reynolds Number		
Pr	Prandtl Number		
P	Pressure [Pa]		
L	Length [m]		
f	Friction Factor		
v	Velocity [m/s]		
D	Diameter [m]		
μ	Viscosity [Pa s]		
K	Concentrated pressure loss coefficient		
$\dot{m}$	Mass Flow [kg/s]		
V	Volume, Displacement [m^3]		
$\dot{V}$	Volume Flow Rate [m^3/s]		
Δh	Enthalpy difference [kJ/kg]		
Greeks			
α	Solar Height [deg]		
β	Tilt angle [deg]		
ρ	Density [kg/m^3]		

2 System description

The solar power plant system is described in fig. 1 and is the same analyzed in previously published papers [39, 40]. The Heat Transfer Fluid (HTF) is heated in the solar field and sent to the ORC module. As heat transfer fluid, pressurized hot water was chosen because of its high conductivity and specific heat and therefore for the highest heat removal capacity. Since the maximum temperature of the HTF was \ang{160} C, a maximum working pressure of 8 bar was considered to prevent fluid evaporation in the solar field. The choice of this pressure is not a problem for the solar field, being much lower than that of similar systems reported in the literature [41]. The ORC module consists of an evaporator, a rotary positive displacement expander, an internal heat exchanger and a dry air condenser. The working fluid was R600a, because of the good results obtained in a previous steady-state analysis [40], due to two principal factors:

- the value of the expander built-in volume ratio, which was close to the volume ratio of the working fluid at the design point;
- the high vapor density of R600a, which makes the use of a positive displacement expander really convenient, because of the small volume flow rate.

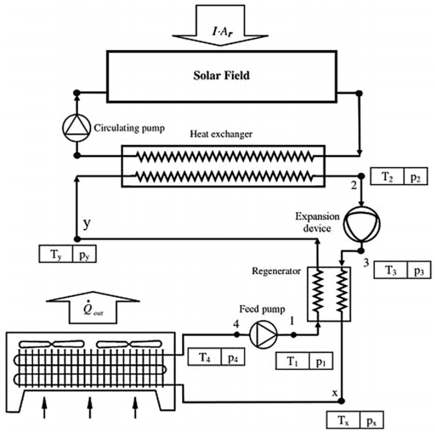

Figure 1: *Scheme of the plant and T-s diagram of the cycle.*

The maximum evaporating pressure of the working fluid was limited to 28.4 bar, corresponding to a saturation temperature of \ang{120} C, following the reccomendation of limiting the evaporating temperature 10 or 15 °C below the critical point to prevent unstable operation, as suggested in [42]. Operation at this pressure level is not an issue, being this value below 30 bar, the maximum pressure reccommended for an ORC [43].

An internal heat exchanger was introduced to recover the sensible heat after the expansion. No storage system was employed in the plant, due to the high flexibility of the positive displacement expander, which can operate at different pressure ratios and rotary speed. Despite the variable power output, the lack of a storage system allows to operate with a solar multiple of 1: the collector field can be designed at the maximum thermal power of the ORC module and does not need oversizing. In this way, plant cost and complexity can be lower than that required when equipping the plant with a storage system.

3 Numerical model

The numerical model was developed with the simulation tool AMESim, and is the same described in the previous paper [39]. For the sake of completeness, a brief description of the model and its simplified scheme (fig. 2) are reported.

3.1 Solar Field

CPCs collectors were modeled in order to take into account all the main heat transfer process, according to fig. 3 and tab. 1.

For the sake of simplicity, only one row of collectors was modeled and the mass flow rate was then multiplied by the number of rows. The inertia, as well as pressure drop and thermal losses of the HTF fluid inside the pipes of the collectors was taken into account. The heat transfer inside the pipe was evaluated according to the Sieder and Tate correlation, which provided the Nusselt number:

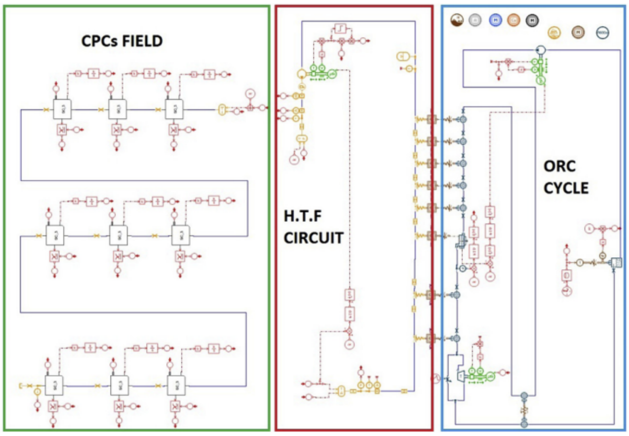

Figure 2: *Numerical model of the system.*

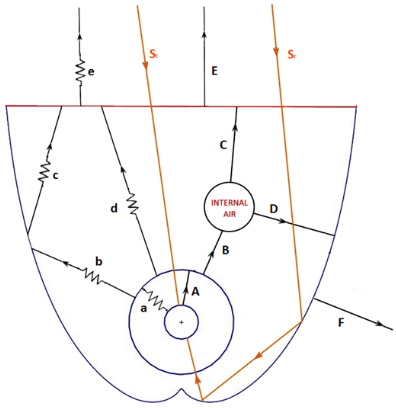

Figure 3: *CPC thermal exchange.*

$$Nu = \begin{cases} 1.86 \cdot (Re \cdot Pr)^2 \cdot \left(\frac{\mu}{\mu_w}\right)^{0.14} & Re < 10000 \\ 0.027 \cdot Re^{0.8} \cdot Pr^{0.33} \cdot \left(\frac{\mu}{\mu_w}\right)^{0.14} & Re \geq 10000 \end{cases} \tag{3.1}$$

Pressure drop was instead calculated according to the formulation of Darcy-Weisbach:

$$\Delta P = f \cdot \rho \cdot L \cdot \frac{v^2}{2 \cdot D_{hyd}} \tag{3.2}$$

where f is the friction factor, and D_{hyd} is the hydraulic diameter of the pipe, which for the commercial evacuated pipes was 10 mm. The friction factor was evaluated according to the Colebrook formulation.

Radiative Exchange		Convective - Conductive Exchange	
Receiver-external evacuated pipe envelope	a	Convection inside the evacuated pipe	A
External evacuated pipe-reflector	b	Convection between External evacuated pipe and internal air	B
Reflector-glass cover	c	Convection between Internal air and glass cover	C
External evacuated pipe-glass cover	d	Convection between internal air and reflector	D
Glass cover-sky	e	Convection between glass cover and ambient	E
Solar radiation input	S_r	Conduction between reflector and insulator	F
		Conduction between evacuated pipe and receiver	Not reported in fig. 3
		Convection between receiver and H.T.F. fluid	Not reported in fig. 3

Table 1: *CPC thermal exchange mechanisms.*

Solar irradiation input on the collectors tilted of an angle β was evaluated by data of ground radiation with the equation:

$$G = I_{bn}\cos(i) + \frac{I_{do}}{C}\cdot\cos^2\left(\frac{\beta}{2}\right) + (I_{bn}\sin(\alpha) + I_{do})\cdot r\sin^2\left(\frac{\beta}{2}\right) \tag{3.3}$$

$$\cos(i) = \cos(a - a_c)\cdot\cos(\alpha)\cdot\sin(\beta) + \sin(\alpha)\cdot\cos(\beta) \tag{3.4}$$

considering direct radiation as the only component of the solar radiation.

The effect of the concentrator acceptance angle was modelled by cutting off radiation data out of the range of the acceptance angle.

Mutual shading between rows was included in the model by evaluating the distance and therefore the shading angle between the rows.

The numerical model of the collectors was calibrated and modelled according to the procedure described in [5] taking into account the real curve declared by the manufacturer of evacuated pipes (fig. 4). These collectors were the same named with the letter B in the previous steady-state preliminary analysis [40]. To calibrate the heat capacity of the collectors, experimental tests in dynamic conditions were carried on a prototype built at the D.E.S.T.eC. department of the university of Pisa: the calibration and validation of the transient behavior of the collector model is reported in [46].

3.2 HTF circuit

The HTF circuit was modelled as an open loop, which received the HTF heated from the solar field. The mass flow rate of the HTF was multiplied by the whole number of arrays of the solar field. Within the loop the HTF heated the working fluid of the ORC that was sent back to the solar field by means of a variable speed circulating pump, to control the solar field outlet temperature with a proportional control. The pressure loss of the circuit was taken into account through various punctual orifices, in order to reduce system complexity

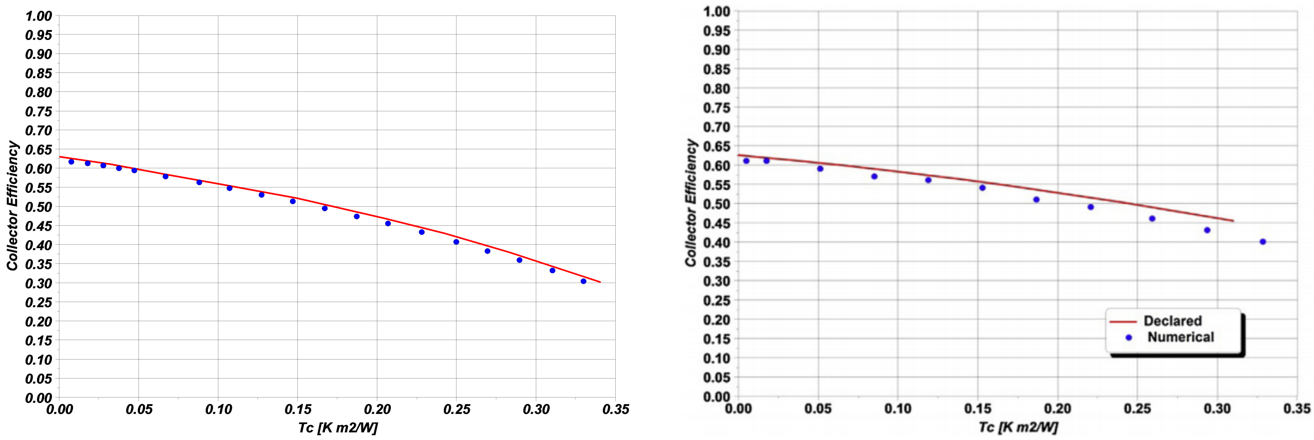

Figure 4: *Collectors efficiency curves: C=1.25 (left), C=2 (right).*

and saving simulation time. These orifices provided the same pressure loss of all the distributed losses of the circuit and of the concentrated loss. The total concentrated loss was evaluated through the following equation:

$$\Delta P = f \cdot \rho \cdot L \cdot \frac{v^2}{2 \cdot D_{hyd}} + \sum_{i=1}^{n} k_i \cdot \rho \cdot \frac{v^2}{2} = K \cdot \rho \cdot \frac{v^2}{2} \tag{3.5}$$

where k_i is the loss coefficient for the generic concentrated pressure loss and K is the equivalent concentrated loss coefficient of the circuit.

For the circulating pump the model of an ideal positive displacement pump was considered. The mass flow rate elaborated by the ideal pump was computed as

$$\dot{m} = \rho \cdot V \cdot \frac{n}{60} \tag{3.6}$$

A constant isentropic efficiency of 0.8 was considered for thisdevice.

3.3 ORC module

Concerning the modeling of the ORC module, heat exchangers were modelled using two different correlations for the HTF side and for the ORC side:

- HTF side calculated the Nusselt number through the Sieder and Tate correlation [44];
- Organic fluid side calculated the heat transfer coefficient using the VDI correlation for horizontal pipes [44]: since the software did not have any correlation to model the shell of the heat exchangers, additional chambers were inserted into the model to take into account the shell volume, which from calculation

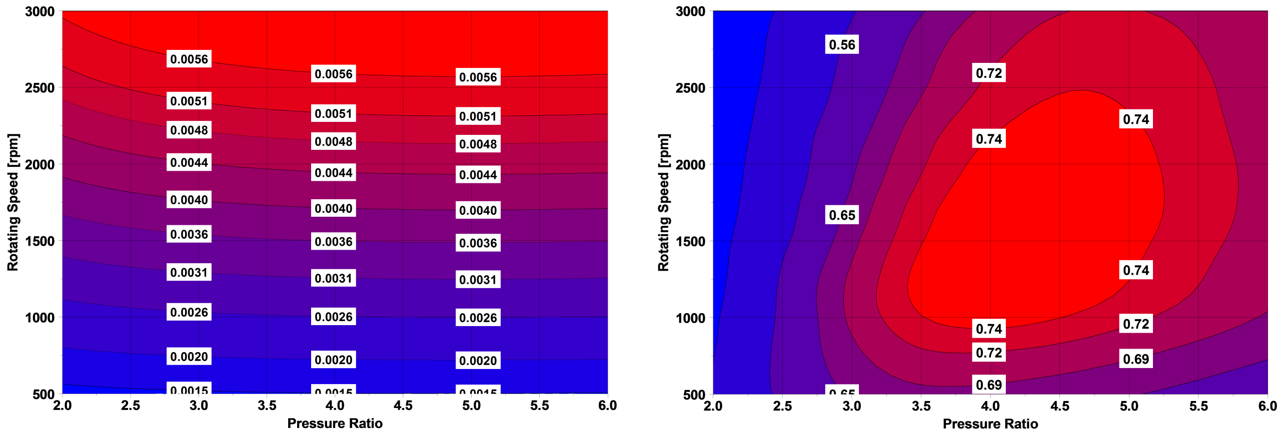

Figure 5: *Expander maps: volume flow rate (left) and isentropic efficiency (right).*

was expected to be about 100 liters.

The expander was modelled using the submodel of a generic turbine: the rotary expander behavior was taken into account by interpolating look up tables of volume flow rate and isentropic efficiency. These data were calculated through a numerical model of the expander and were presented in previous papers [21, 22]. The model of the expander was calibrated with the experimental results from the test campaign on the prototype of the Wankel expander developed at the D.E.S.T.eC. department of the University of Pisa: the comparison between the experimental data and simulation results are reported in [21, 22]. From this data the code evaluated the expander power as:

$$\dot{W} = \rho_{ad} \cdot \dot{V} \cdot \Delta h_{is} \cdot \eta_{is} \tag{3.7}$$

The operating maps of the expander are reported in fig. 5, as a function of pressure ratio and expander rotating speed.

For the sake of simplicity, internal heat exchanger (IHE) was modelled as an ideal exchanger with an imposed constant efficiency. The value of this parameter is very important: if from one hand a high IHE efficiency lead to the increase of the cycle thermal efficiency, from the other cause an increase of the temperature of the HTF at the solar field inlet, decreasing the solar field efficiency. A sensitivity analysis on this parameter was carried, simulating the plant in the same five days of the previous work [39], for different collectors concentration factors (C=1.25 and C=2), and for various values of the set point for the evaporating pressure and the superheating grade.

As from fig. 6, the plant specific production for unit of concentrators aperture area, increased with the IHE efficiency for all the thermodynamic and solar field configurations tested. For this reason, the efficiency of 0.85 was considered in this analysis.

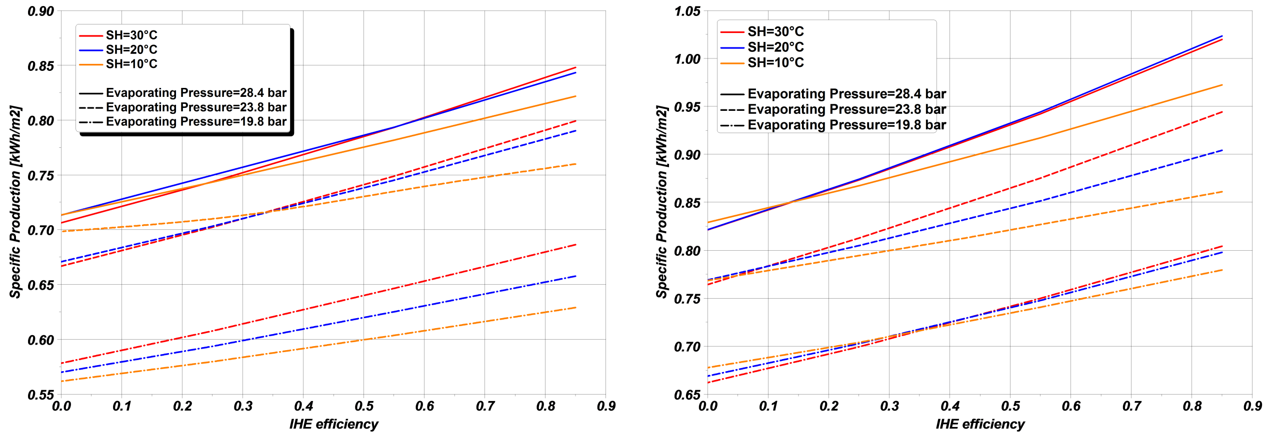

Figure 6: *Effect of the IHE efficiency on specific production for C=1.25 (left) and C=2 (right).*

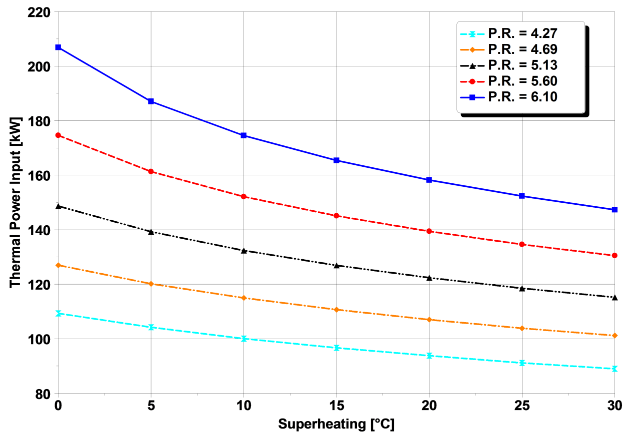

Figure 7: *ORC module thermal power input as a function of superheating grade and pressure ratio.*

The air cooled condenser was modelled as a chamber at a temperature 15°C higher than the ambient: in this way the condensing temperature varied through the simulation, taking into account of the ambient temperature variations; fan consumption was calculated by multiplying the heat rejected to the condenser by the specific consumption of the fans. A value of 17 W/kW$_{th}$ was retained for the simulations, which is a typical value obtained from manufacturers catalogs.

The variation of the evaporating pressure or of the superheating temperature produces a different production and a different amount of exchanged heat. Fig. 7 shows that exchanged thermal power increases with evaporating pressure but decrease with the superheating temperature. The number of collectors was therefore varied in order to provide the maximum allowable thermal power to the ORC module on the day with the highest radiation intensity of the year, for each thermodynamic condition, retaining the solar multiple equal to 1.

3.4 Control loops

A sliding-velocity control strategy was adopted. The outlet temperature of the solar field, as well as the evaporating temperature and the superheating temperature were kept constant by the control system during operation. Three control loops were adopted to this purpose:

- Collector field outlet temperature controlled by varying the velocity of the circulating pump;
- Evaporating pressure controlled by varying the velocity of the rotary expander in the range between 500 and 3000 rpm.
- Superheating temperature controlled by varying the pump speed.

When the solar radiation begins to warm up the HTF, the circulating pump starts rotating at the minimum speed, warming up the organic fluid into the evaporator. When the HTF reaches the set point value, the pump increases its speed to retain the HTF constant at the set point value. The HTF warms up the organic fluid into the evaporator, increasing the pressure and evaporating the organic fluid. When the pressure ratio is higher than one, and when the vapor quality is higher than 0.7, the rotary expander begins to rotate to its minimum speed: in this way, due to the flexibility of the volumetric expander, the plant is able to produce power even when the pressure ratio is very low and far from the design point. When the pressure into the evaporator rises up near the set point value, the controller increases the expander velocity in order to retain the pressure constant. In the case of a decrease of the solar radiation, due to a cloud passage, the control system reduces the velocity of the expander to retain the set point. If the decrease of radiation is high (cloudy weather or end of the day), the speed of the rotary expander is reduced to its minimum speed until the pressure ratio remains positive and the vapor quality higher than 0.7.

The calibration of the plant and its behavior in real radiation conditions was analyzed and discussed in the previous paper [39].

3.5 Meteorological data

As reported above, three different sites were considered: northern Italy, in the district of Milan; central Italy, in the district of Pisa; southern Italy, in the district of Ragusa, in Sicily. Hourly discretized radiation and ambient temperature were the input of the numerical model. Data were evaluated from historical series according to the standard [45]. The radiation trend, hourly discretized, and its average monthly value are reported in fig. 8 for the three places.

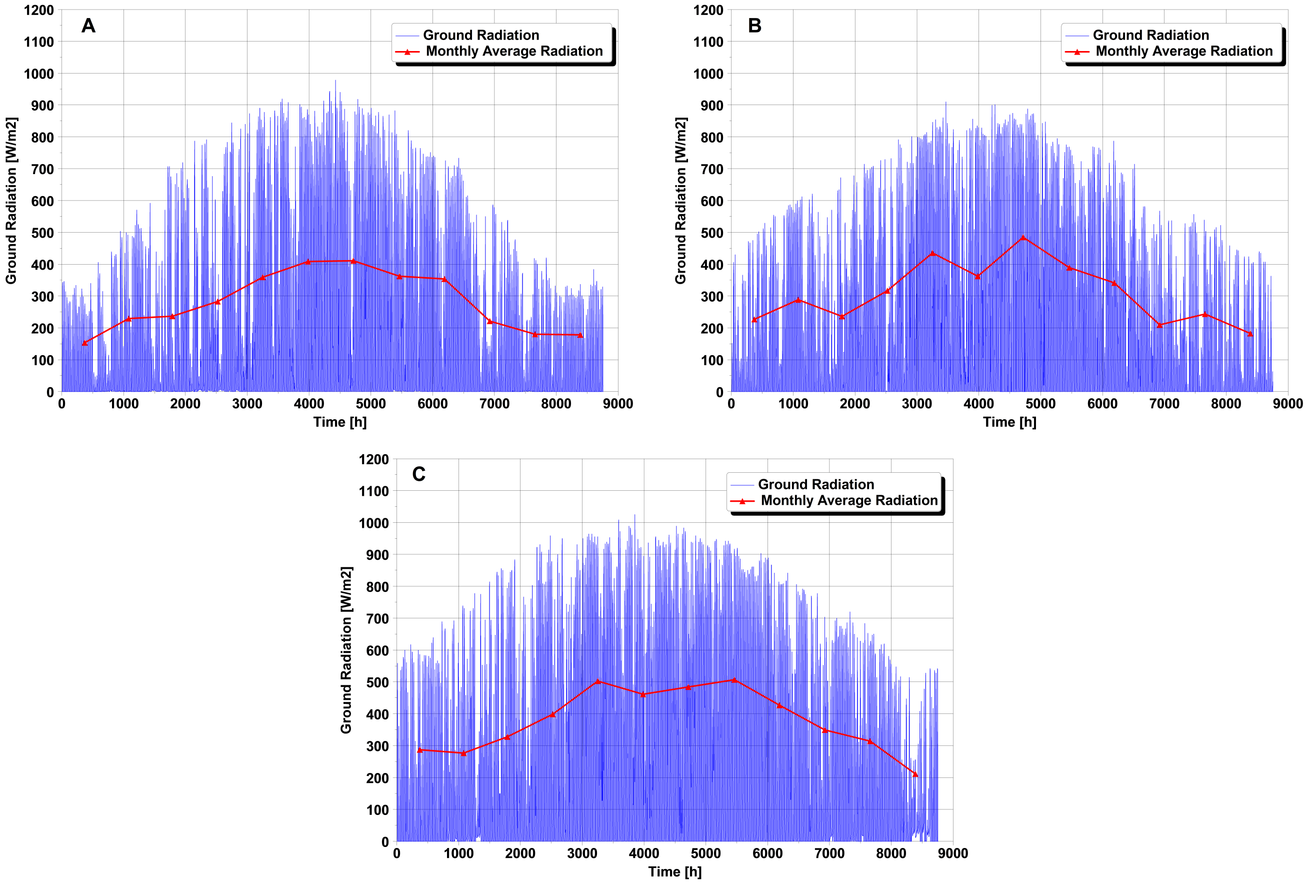

Figure 8: *Ground Radiation for the three district: A Northern Italy, B Center Italy, C Southern Italy.*

4 Results

In this paragraph, the annual production of the plant in the three sites is analyzed and compared through the analysis of the maps of specific production per unit of panel surface. Maps were defined as a function of the set point values of superheating temperature and evaporating pressure: in this way, the optimal setting of this two values can be evaluated for each solar field conditions. The set point of solar field outlet temperature was varied with the superheating temperature, retaining constant the approach point to 10°C.

4.1 Dynamic model behavior

Different values for superheating grade, evaporating pressure, solar field concentration ratio and tilt angle were compared. The analysis of the annual production was obtained dividing the annual simulation in twelve sub-simulation, one for each month of the year. Fig. 9, 10 and 11 reported the maps of specific production per unit of panel surface for the three localities, for both the two analyzed concentration factors (C=1.25 and C=2) and for different tilt angles. The maximum and the minimum value for the tilt angle was determined by the maximum and minimum solar height for which the sun was visible from the concentrators, due to their acceptance angle. For this reason, when operating with C=2, the minimum tilt angle considered was 25°, corresponding to a minimum solar height of 35°: in this configuration the sun was not visible by the solar field until it reached the solar height of 35°. For lower values of tilt, this value increased, reducing the captured radiation. Conversely, the maximum tilt angle considered was 45°: in fact, when operating with C=2, the maximum solar height visible by the concentrators in this configuration was 70°, which is also about the maximum solar height for the localities considered in this study. Higher values of the tilt would have led to the lack of sun visibility during the central hours of the days around the summer solstice, causing an unacceptable cooling down of the plant in the middle of the day.

As expected maximum production was obtained for the southernmost locality, because of the higher incident radiation (fig. 8): in this locality, maximum production was about 1.42 and 1.34 times higher than the maximum production obtained in Pisa with C=1.25 and C=2 respectively. Pisa and Milan provided almost the same annual production, despite the slightly higher value of Pisa.

Specific production for unit area aperture increased both with evaporating pressure and with superheating. The optimal values of these two parameters were 28.4 bar (corresponding to an evaporating temperature of 120°C) and 30°C, for all the three localities, for all the tilt angle and for both the concentration factors. The main reason of this behavior was due to the different extension of the solar field and therefore of the plant thermal inertia. When operating with S.M.=1, the increase of the superheating temperature set-point involved a decrease in ORC thermal power input and therefore in the number of collectors and in system inertia (fig. 7), which was the responsible of the specific production increase with the superheating grade. As an example, the HTF temperature trend and the results of the calculation obtained for five consecutive days of January in Pisa were reported in fig. 12.

From the analysis of fig. 12, the plant started the production when the average solar field temperature was quite low (about 40°C). Conversely, during the shut-down, production stopped when the average solar temperature was at about 50°C. This was due to the difference in the solar field outlet temperature between the start-up and at shut-down: during start-up, in fact the outlet temperature of the solar field was higher than during the shutdown, because of the irradiation power from the sun, allowing the plant to start the production when the average temperature of the solar field was low. The temperature difference indicates that part of the internal energy stored by the solar field during the start-up phase, was not completely recovered during the shut-down. This loss increased with the size of the solar field: decreasing the set-point of superheating grade, the size of the field increased (S.M.=1), causing a larger energy loss. It is worth to notice that this was also the reason for which the highest values of specific production were obtained with collectors having C=2. In fact, from the definition of concentration ratio:

$$C = \frac{A_c}{A_r} \tag{4.1}$$

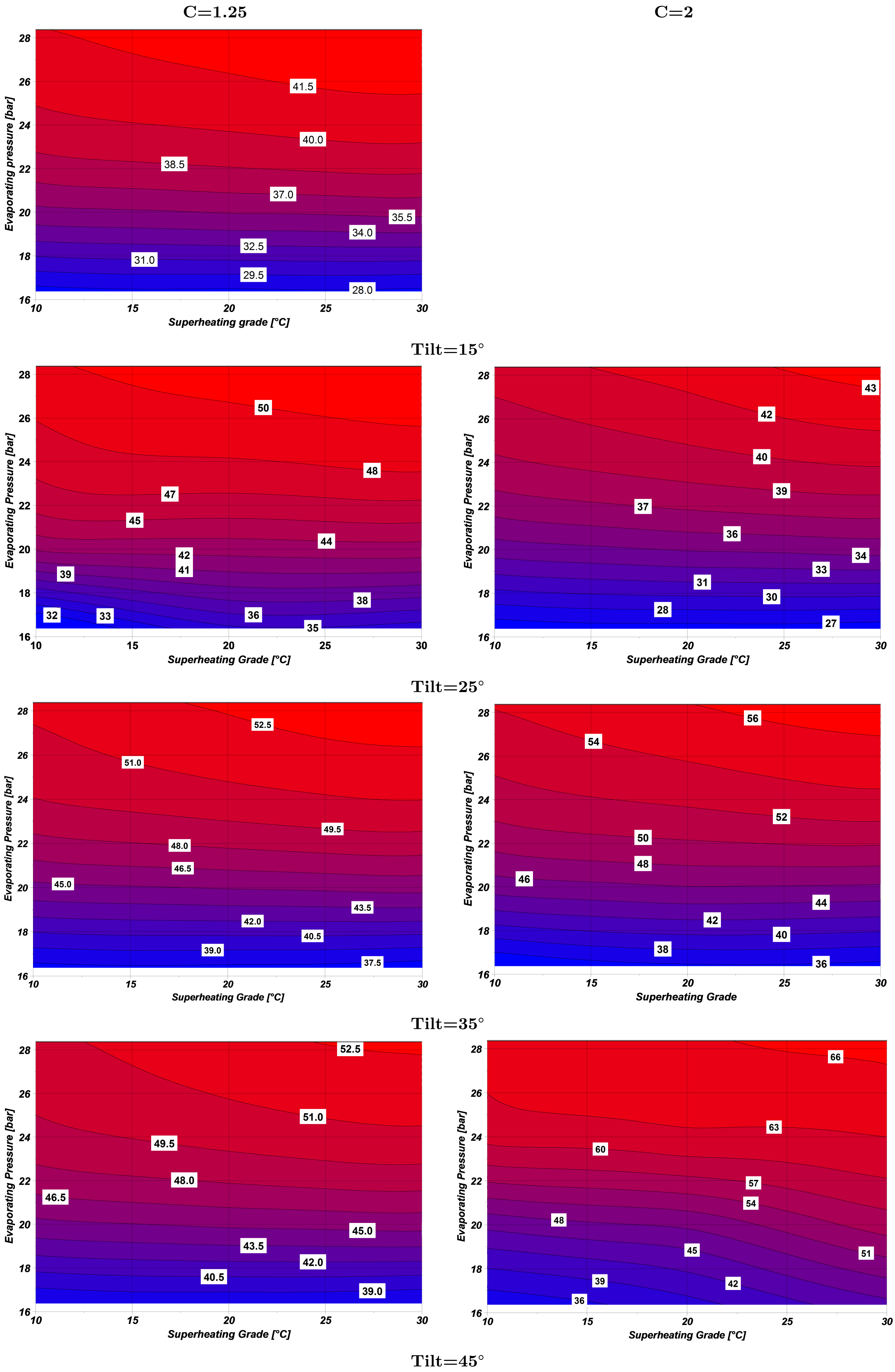

Figure 9: *Maps of specific production [kWh/m^2](Milan).*

C=1.25 **C=2**

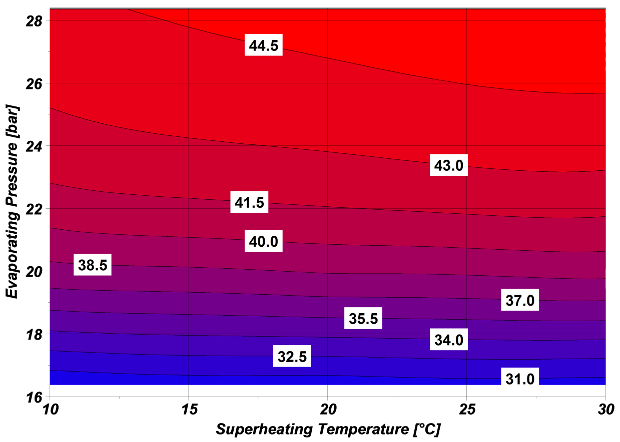

Tilt=15°

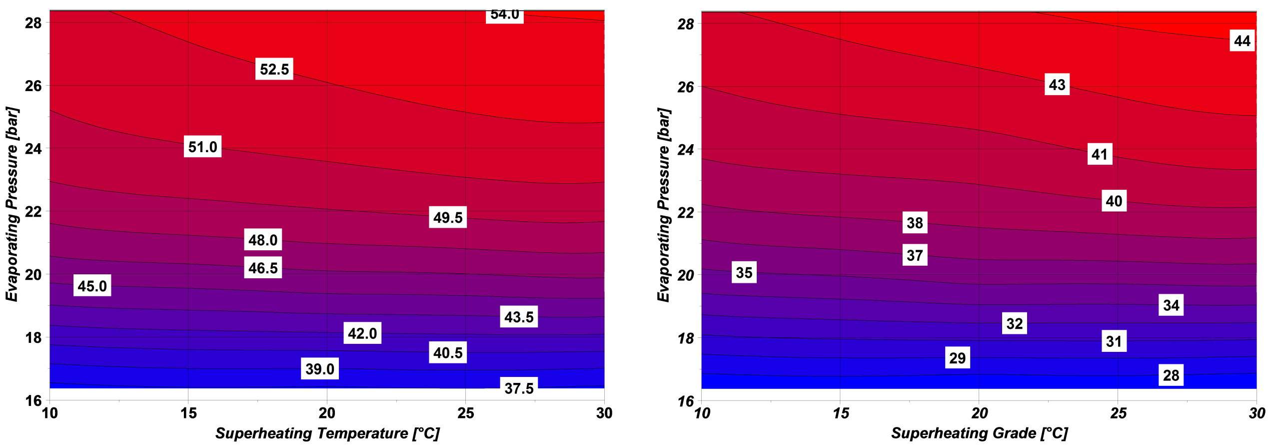

Tilt=25°

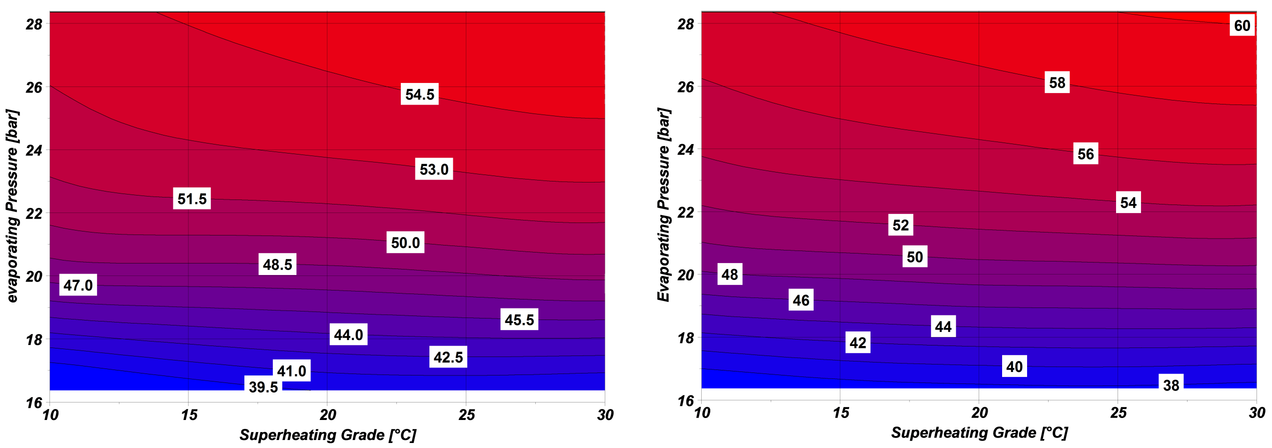

Tilt=35°

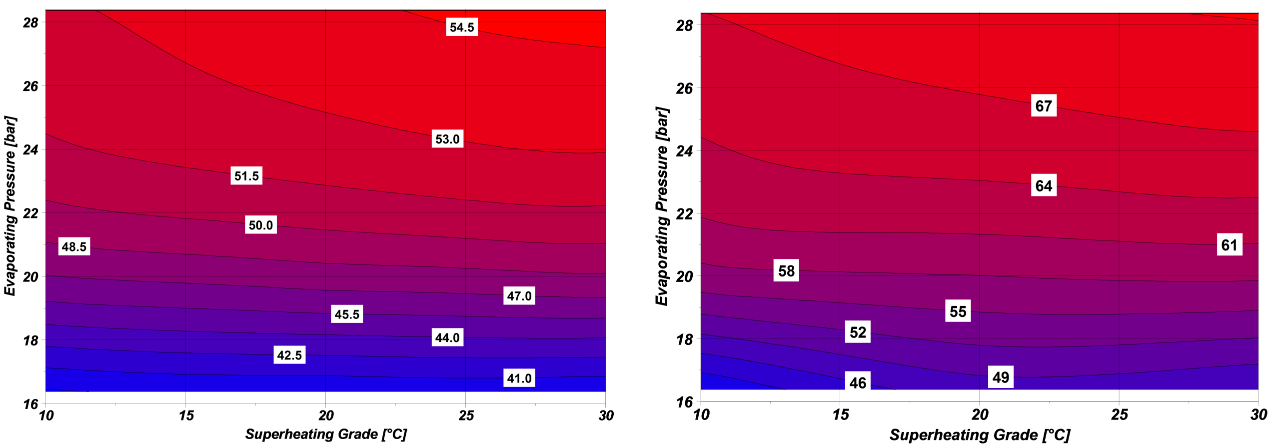

Tilt=45°

Figure 10: *Maps of specific production [kWh/m^2](Pisa).*

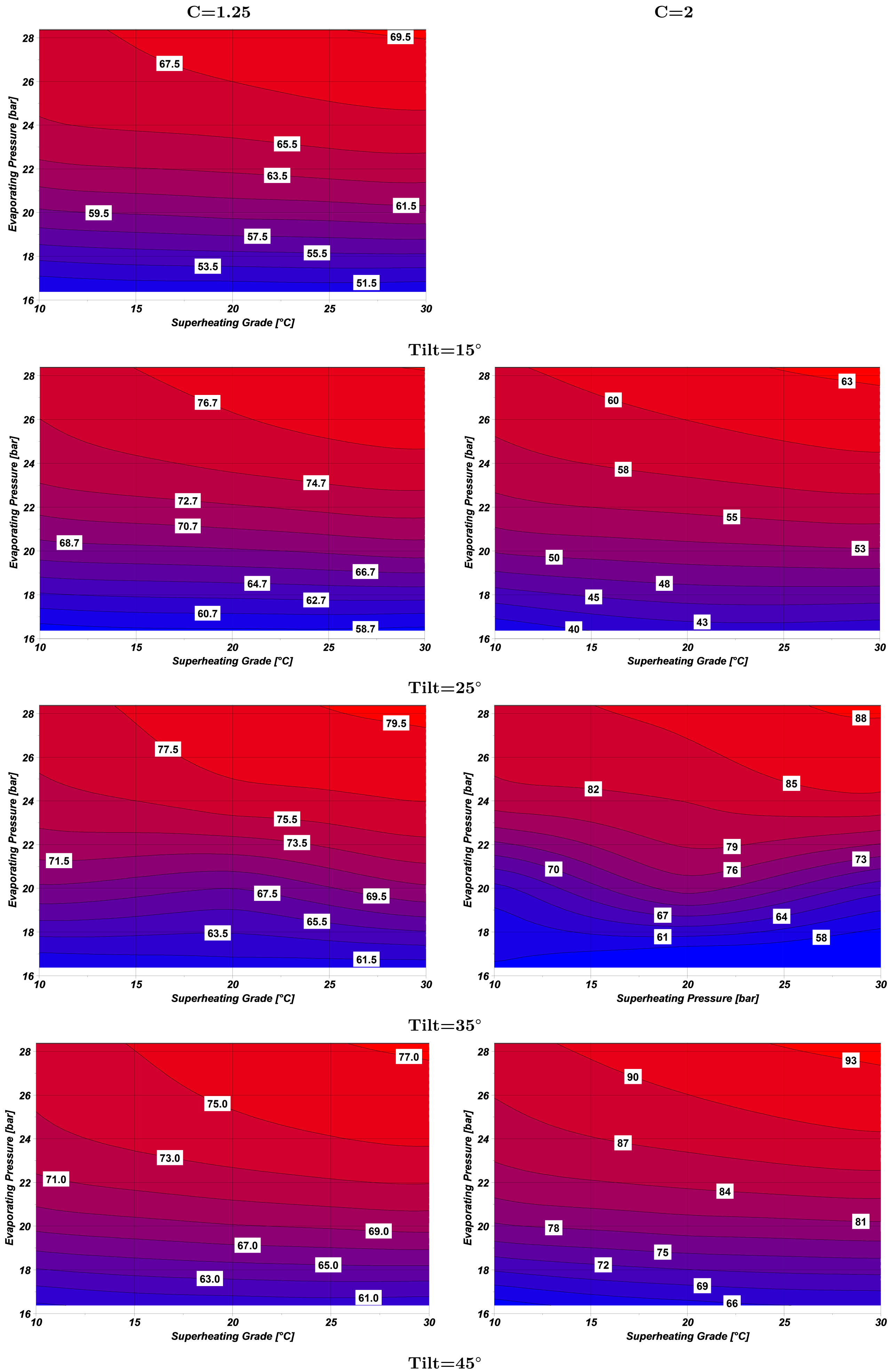

Figure 11: *Maps of specific production [kWh/m^2](Ragusa).*

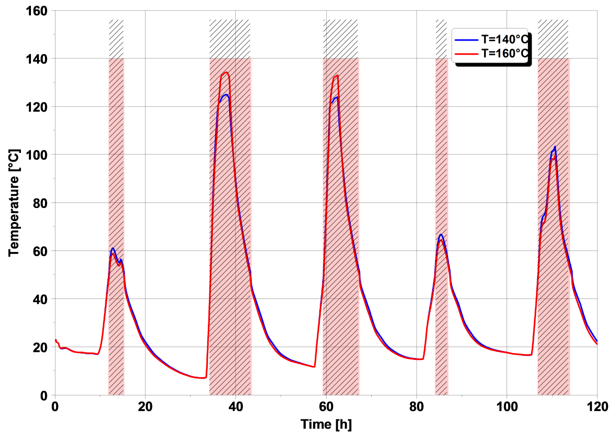

Figure 12: *Trend of the HTF average temperature for two different superheating temperature during five consecutive days of January (Pisa). The pink highlighted area represents the production time for the lower temperature case and the hatch the production time for the higher temperature configuration.*

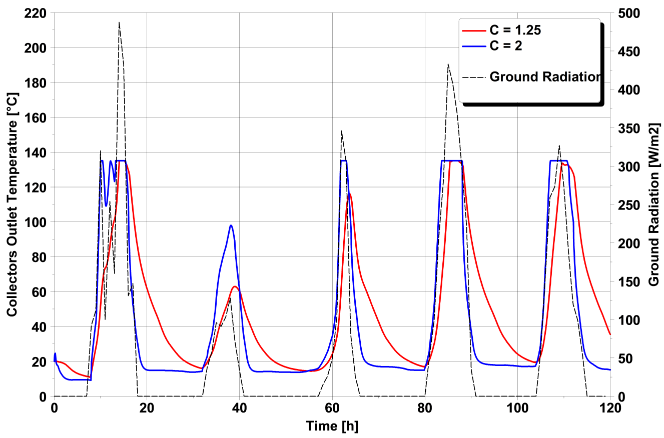

Figure 13: *Comparison of the HTF temperature at solar field outlet between C=1.25 and C=2*

the receiver surface, and therefore the number of collectors with C=1.25 was almost twice the number of collectors with C=2, implying that also the solar field inertia was almost twice the configuration with C=1.25. Because of the lower inertia, the temperature at the solar field outlet was higher for a longer operating time, especially in partly clouded days (fig. 13).

Regarding the evaporating pressure, higher was its set point higher was the plant specific production. In fact, if from one hand, operation at low evaporating pressure required a low number of collectors, reducing the solar field inertia, from the other it reduces the ORC power input: this last component has a constant inertia, due to the fixed volume of the heat exchangers. The reduction of the solar field size increased the time requested to warm up the ORC module, causing the operation at lower pressure during start-up, cool-down and partly clouded days (fig. 14), and reducing the average ORC efficiency. For this reason high values for pressure set point allowed to obtain the highest values of specific production.

The influence of the tilt angle on specific production, evaluated at optimal thermodynamic conditions is reported in fig. 15. When the tilt angle was larger than 30°, collectors with C=2 provided the highest specific

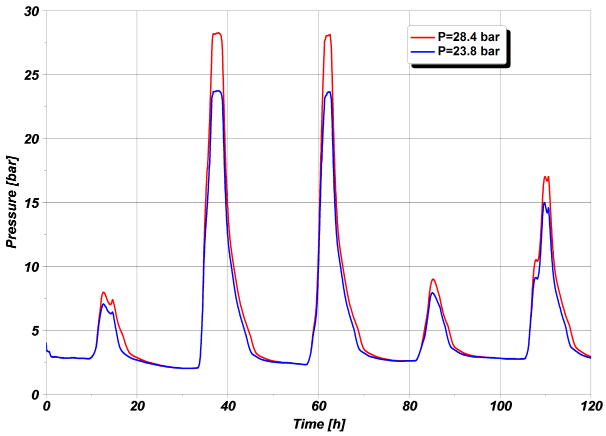

Figure 14: *Effect of the set point of evaporating pressure.*

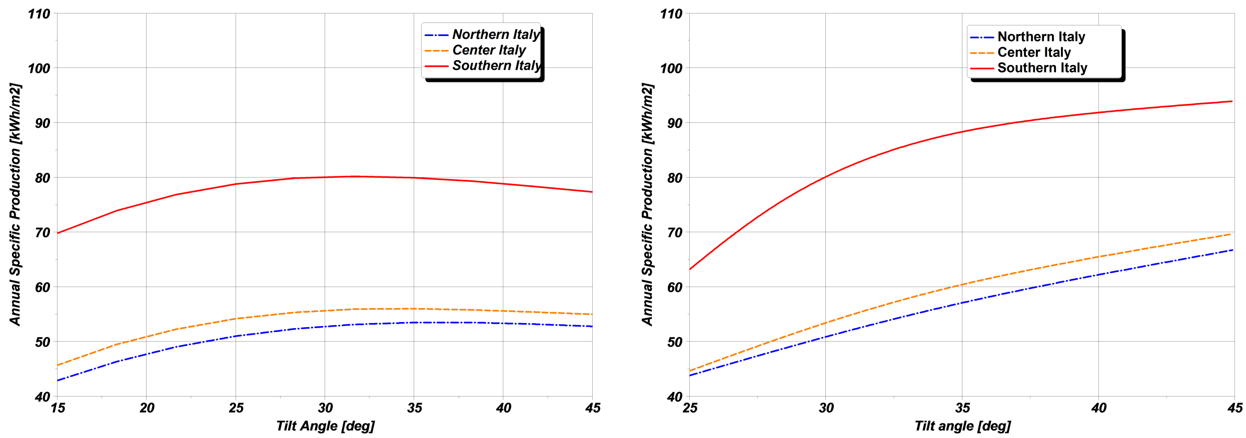

Figure 15: *Specific production as a function of the tilt angle at optimal thermodynamic conditions.*

production. The value of the tilt angle which maximized the specific production depended on latitude, when operating with collectors having C=1.25: 32.5° for Ragusa, 35° for Pisa and 37.5° for Milan. This result was expected, due to the higher average solar height of the southernmost sites. With collectors having C=2, instead the value maximizing the specific production was 45° for all the considered localities: due to the low acceptance angle, the high tilt allowed to reduce the minimum angle for which the receiver saw the sun, increasing the plant operating hours. A secondary effect, which lead to this result, was also represented by the different dynamic of the system at different tilt: in fact, a high tilted panel allowed receiving the solar ray with a better incidence angle at the beginning and at the end of the day, with a faster warm up and a slower cool down (fig. 16).

4.2 Comparison with the steady-state model

In this section, the results obtained in dynamic conditions are compared with those obtained from a steady-state model of the plant. The steady-state model was described in a previous paper [20], computing the average radiation with the Liu and Jordan method and taking into account the actual behavior of the ORC

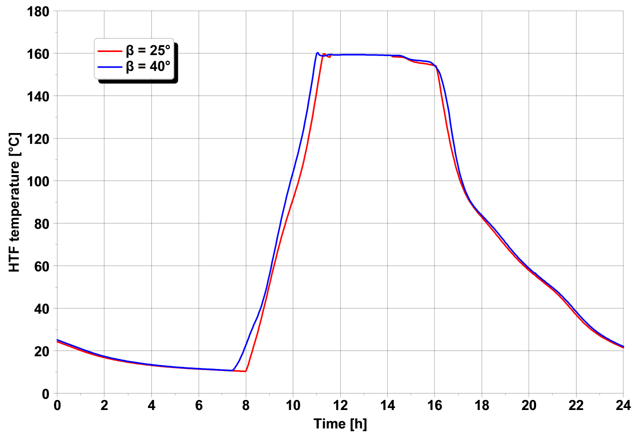

Figure 16: *HTF temperature at collectors field outlet adopting collectors with two different values of tilt angle.*

module with the rotary expander. Maps of specific production obtained in steady-state conditions are reported in fig. 17- 19 for the three localities.

From the comparison of the plant working maps, it is obvious that the two models lead to two different solutions. The difference is particularly evident when low concentration collectors were adopted. The first difference is in terms of energy output: the ratio between the maximum energy output evaluated in steady-state conditions and in dynamic conditions ranged between 1.51 (Milan) to 1.80 (Ragusa) with panels having C=1.25, and between 1.19 (Milan), to 1.49 (Ragusa) with C=2. The reason of this discrepancy was due, first of all to to the effect of the plant inertia which obviously was not considered by the steady-state calculation. It is not a chance that with C=2 the difference of the ratio between the energy output predicted by the steady-state and by the dynamic model was lower than in the case with C=1.25: in this last case, in fact, a larger number of collectors (almost twice) were necessary to operate at S.M.=1 and inertial effects had an important role, due to the amount of fluid stored in the various branches of the solar field. In the maps evaluated in steady-state conditions (fig. 17, 18 and 19), the maximum of specific production tended to shift towards lower values of evaporating pressure and superheating with the tilt angle. In fact, increasing the tilt, the maximum of energy production shifted from summer towards winter, when, due to the lower ambient temperature and radiation intensity, the solar field required lower operating temperatures to keep high efficiency. Both in steady-state and in dynamic conditions, the optimal thermodynamic parameters influenced the overall efficiency, which was the product of the solar efficiency by the ORC module efficiency, and solar collectors efficiency is a function of the collectors temperature, ambient temperature and radiation intensity. In dynamic conditions, this parameter was also influenced by the solar field inertia, which behaves as a resistance during warm-up and as heat source during plant cool-down. If the solar field was concentrated in a point and was not affected by thermal losses, the internal energy accumulated during the warm-up phase would be fully recovered during the plant cool-down. Due to the solar field extension and to the thermal losses, part of the stored internal energy was lost. This loss increases with the solar field dimension.

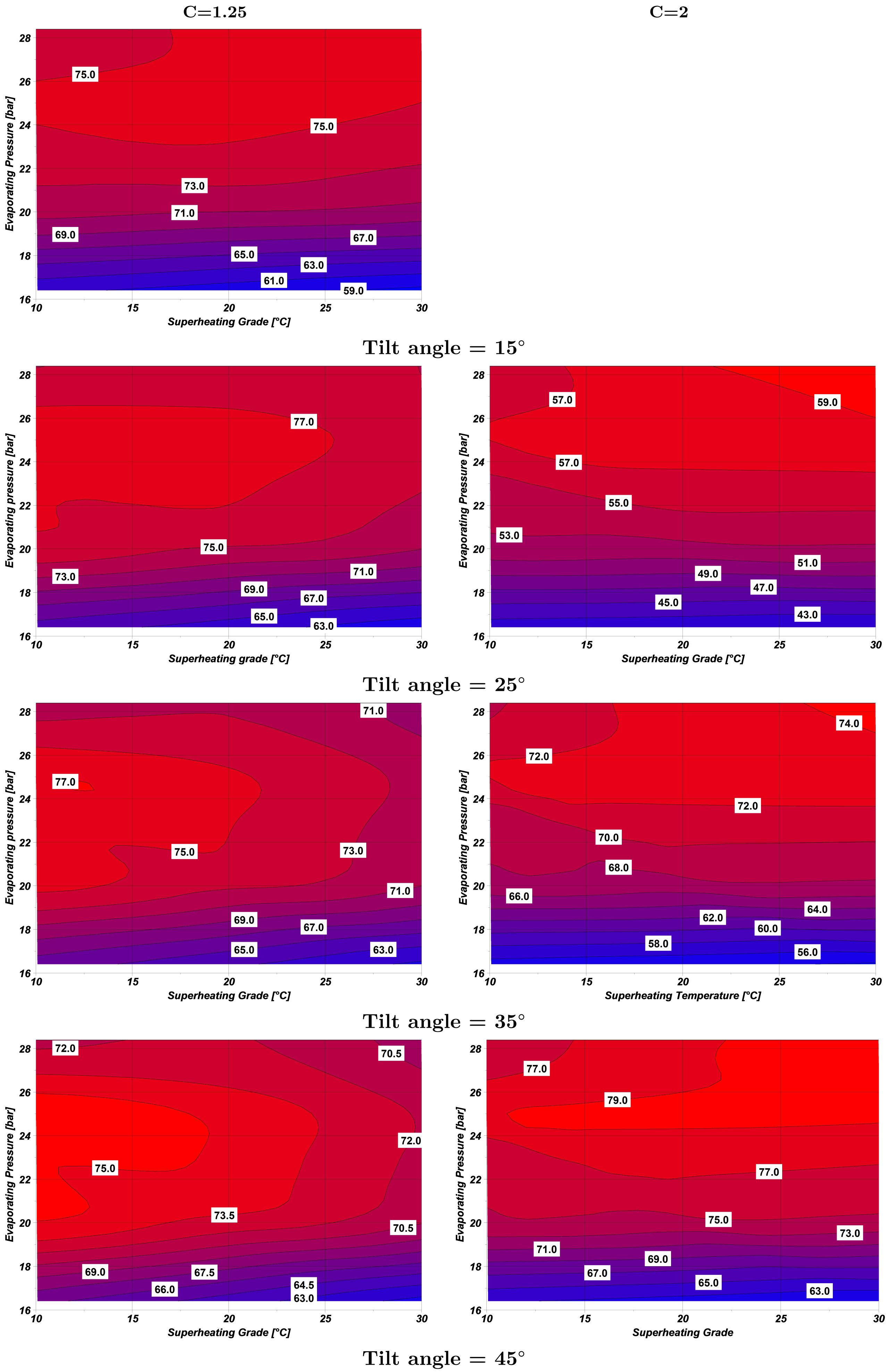

Figure 17: *maps of specific production [kWh/m^2] Milan (steady-state).*

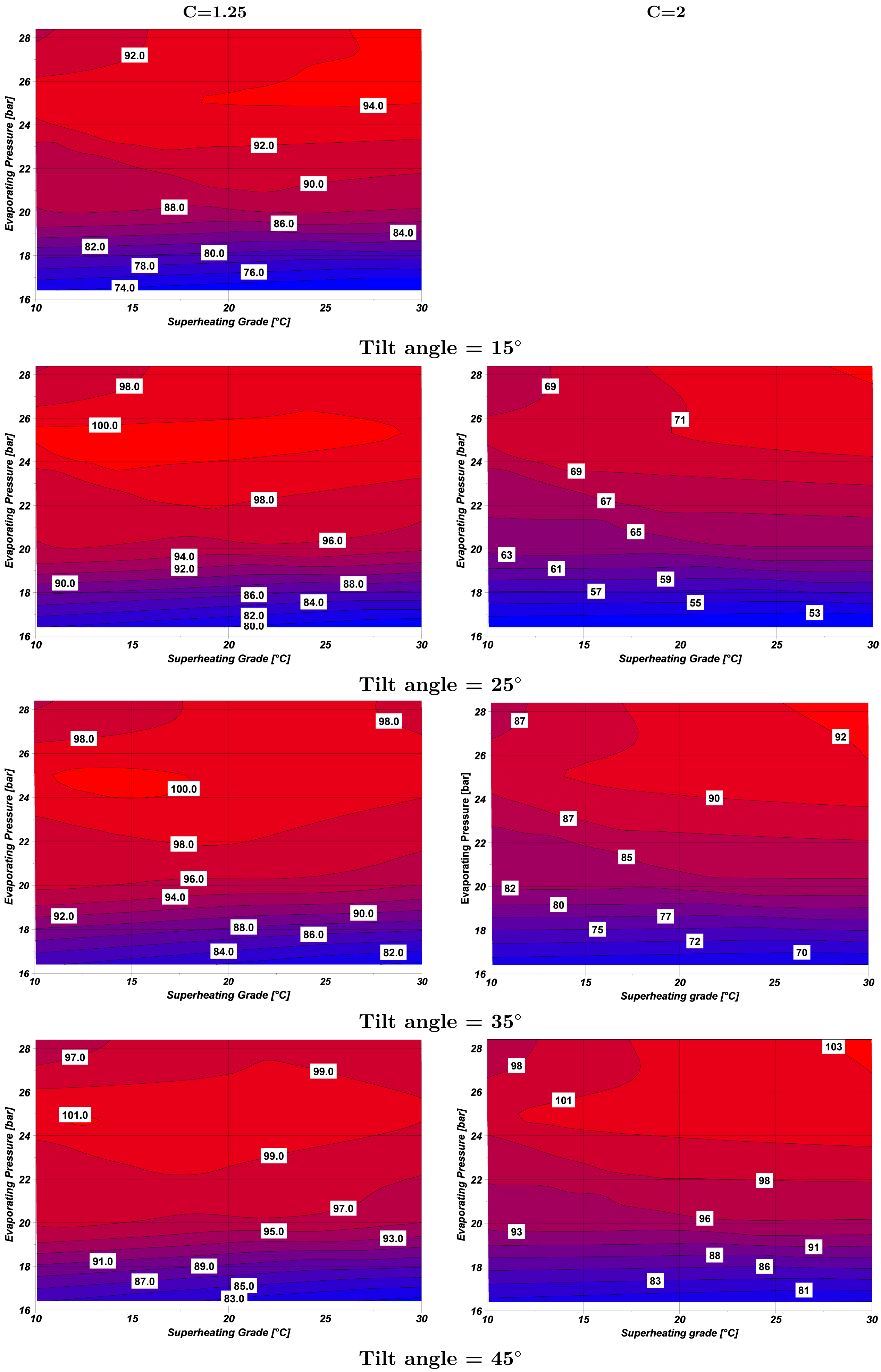

Figure 18: *maps of specific production [kWh/m^2] Pisa (steady-state).*

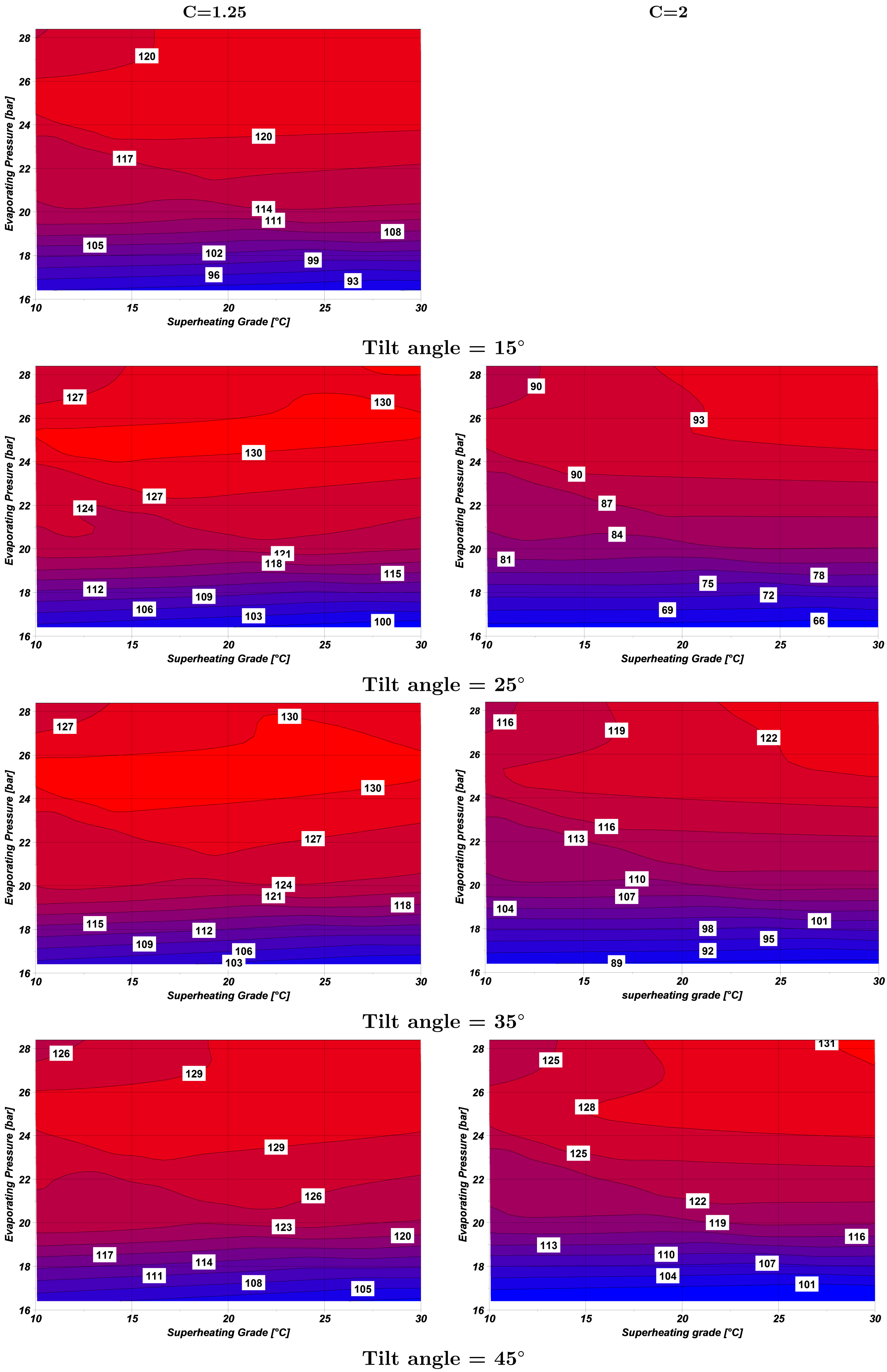

Figure 19: *maps of specific production [kWh/m^2] Ragusa (steady-state).*

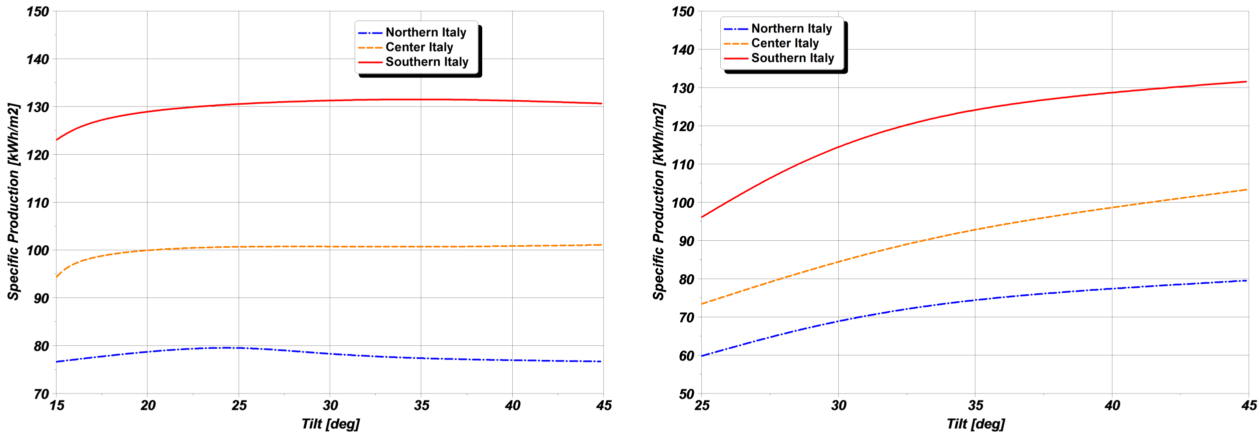

Figure 20: *Effect of the tilt angle in steady-state conditions.*

Regarding the influence of the tilt angle (fig. 20), with collectors having C=1.25 optimal values predicted by the steady-state model were lower than those predicted by the dynamic model. The steady-state model in fact, took into account the diffuse radiation: the optimal tilt angle should be lower in those localities where diffuse radiation is particularly high (this is the case of Milan). For Ragusa, where diffuse radiation is very low, if compared to the direct radiation, the two models gave almost the same results. With C=2, instead, the two models predicted the same optimal tilt value for all the three localities considered. At higher concentration, in fact, the role of the diffuse radiation decreases, as well as the impact of the thermal inertia of the solar field. The dynamic model was essential for understanding the behavior of this plant with no thermal storage and with a sliding velocity control of the ORC module and also allowed to highlights some aspects which could not be taken into account by the steady-state model, whose definition criteria should be revised, at least when operating with low concentration factor collectors. The control strategy proved to be suitable in reducing solar field extension and therefore saving costs, especially for high concentration ratio, where the losses due to the solar field inertia were low.

Conclusion

In this work, the dynamic production of a small-scale solar power plant with compound parabolic collectors and ORC module has been analyzed. The sliding-velocity control strategy, together with the high flexibility of the rotary expander, allowed the plant to operate without the need of a thermal storage, i.e. with S.M. equal to 1. The system has been simulated for a year-long operation, using hourly-discretized data and in three different sites in Italy: Milan, Pisa and Ragusa. Results indicated that specific production decreased with latitude and increased with concentration factor: this last effect was due to the lower size of the solar field and therefore to the lower loss associated to the plant inertia. Simulations indicated that a superheating of 30°C and the maximum evaporating pressure of 28.4 bar maximized plant specific production both with

C=1.25 and C=2, and for all the tilt angle: the cause of this behavior was found to be the size of the solar field and the partial capacity of recovering the internal energy of the system.

The comparison with the steady-state analysis reported a certain discrepancy with transient analysis, when low concentration solar collectors were adopted, due to the effect of both solar field and ORC module. With C=2, despite the difference in terms of specific production between the transient and the steady-state analysis, there was a good agreement in terms of values of set point temperature and superheating temperature which maximized system specific production. As for the optimal tilt angle, the trend of specific production was the same for both the steady-state and the transient simulation when the concentration factor was 2. The sliding-velocity control strategy proved to be able to drive the plant without the need of a thermal storage system, especially in those cases where solar field thermal inertia was not too large.

References

[1] J. Li, P. Li, G. Pei, J. Alvi, J. Ji, Analysis of a novel solar electricity generation system using cascade Rankine cycle and steam screw expander, Applied Energy. 165 (2016) 627-638.

[2] R. Rayegan, Y. Tao, A procedure to select working fluids for Solar Organic Rankine Cycles (ORCs), Renewable Energy. 36 (2011) 659-670.

[3] A. Gudekar, A. Jadhav, S. Panse, J. Joshi, A. Pandit, Cost effective design of compound parabolic collector for steam generation, Solar Energy. 90 (2013) 43-50.

[4] A. Rabl, N. Goodman, R. Winston, Practical design considerations for CPC solar collectors, Solar Energy. 22 (1979) 373-381.

[5] J. A. Duffy, W. A. Beckman, Solar Engineering of thermal processes, Fourth Edition (2013) Wiley & Sons Inc.

[6] A. Farouk Kothdiwala, B. Norton, P.C. Eames, The effect of variation of angle of inclination on the performance of low-concentration-ratio compound parabolic concentrating solar collectors, Solar Energy. 55 (1995) 301-309.

[7] Y. Yadav, A. Yadav, N. Anwar, P. Eames, B. Norton, The fabrication and testing of a line-axis compound parabolic concentrating solar energy collector, Renewable Energy. 9 (1996) 572-575.

[8] A. Azhari, H. Khonkar, A thermal comparison performance of CPC with modified (duel-cavity) and non-modified absorber, Renewable Energy. 9 (1996) 584-588.

[9] W. Zheng, L. Yang, H. Zhang, S. You, C. Zhu, Numerical and experimental investigation on a new type of compound parabolic concentrator solar collector, Energy Conversion And Management. 129 (2016) 11-22.

[10] M. Antonelli, M. Francesconi, P. Di Marco, U. Desideri, Analysis of heat transfer in different CPC solar collectors: A CFD approach, Applied Thermal Engineering. 101 (2016) 479-489.

[11] X. Li, Y. Dai, Y. Li, R. Wang, Comparative study on two novel intermediate temperature CPC solar collectors with the U-shape evacuated tubular absorber, Solar Energy. 93 (2013) 220-234.

[12] H. Singh, P. Eames, A review of natural convective heat transfer correlations in rectangular cross-section cavities and their potential applications to compound parabolic concentrating (CPC) solar collector cavities, Applied Thermal Engineering. 31 (2011) 2186-2196.

[13] B. Abdullahi, R. AL-Dadah, S. Mahmoud, R. Hood, Optical and thermal performance of double receiver compound parabolic concentrator, Applied Energy. 159 (2015) 1-10.

[14] J. Wang, Z. Yan, P. Zhao, Y. Dai, Off-design performance analysis of a solar-powered organic Rankine cycle, Energy Conversion And Management. 80 (2014) 150-157.

[15] G. Pei, J. Li, J. Ji, Analysis of low temperature solar thermal electric generation using regenerative Organic Rankine Cycle, Applied Thermal Engineering. 30 (2010) 998-1004.

[16] S. Quoilin, S. Declaye, A. Legros, L. Guillaume, V. Lemort, Working fluid selection and operating maps for Organic Rankine Cycle expansion machines, Proceedings of the International Compressor Engineering Conference at Purdue, July 16-19, 2012.

[17] B. J. Woodland, J. E. Brown, E. A. Groll, W. T. Horton, Experimental Testing of an Organic Rankine Cycle with scroll type expander, Publications of the Ray W. Herrick Laboratories. Paper 52, 2012.

[18] S. Declaye, S. Quoilin, L. Guillaume, V. Lemort, Experimental study on an open-drive scroll expander integrated into an ORC (Organic Rankine Cycle) system with R245fa as working fluid, Energy. 55 (2013) 173-183.

[19] S. Quoilin, V. Lemort, J. Lebrun, Experimental study and modeling of an Organic Rankine Cycle using scroll expander, Applied Energy. 87 (2010) 1260-1268.

[20] S. Clemente, D. Micheli, M. Reini, R. Taccani, Energy efficiency analysis of Organic Rankine Cycles with scroll expanders for cogenerative applications, Applied Energy. 97 (2012) 792-801.

[21] M. Antonelli, A. Baccioli, M. Francesconi, U. Desideri, L. Martorano, Operating maps of a rotary engine used as an expander for micro-generation with various working fluids, Applied Energy. 113 (2014) 742-750.

[22] M. Antonelli, A. Baccioli, M. Francesconi, L. Martorano, Experimental and Numerical Analysis of the Valve Timing Effects on the Performances of a Small Volumetric Rotary Expansion Device, Energy Procedia. 45 (2014) 1077-1086.

[23] M. Orosz, A. Mueller, B. Dechesne, H. Hemond, Geometric Design of Scroll Expanders Optimized for Small Organic Rankine Cycles, Journal Of Engineering For Gas Turbines And Power. 135 (2013) 042303.

[24] M. Ali Tarique, I. Dincer, C. Zamfirescu, Experimental investigation of a scroll expander for an organic Rankine cycle, International Journal Of Energy Research. 38 (2014) 1825-1834.

[25] S. Quoilin, R. Aumann, A. Grill, A. Schuster, V. Lemort, H. Spliethoff, Dynamic modeling and optimal control strategy of waste heat recovery Organic Rankine Cycles, Applied Energy. 88 (2011) 2183-2190.

[26] M. Antonelli, A. Baccioli, M. Francesconi, P. Psaroudakis, L. Martorano, Small Scale ORC Plant Modeling with the AMESim Simulation Tool: Analysis of Working Fluid and Thermodynamic Cycle Parameters Influence, Energy Procedia. 81 (2015) 440-449.

[27] N. Mertens, F. Alobaid, T. Lanz, B. Epple, H. Kim, Dynamic simulation of a triple-pressure combined-cycle plant: Hot start-up and shutdown, Fuel. 167 (2016) 135-148.

[28] W. Al-Maliki, F. Alobaid, V. Kez, B. Epple, Modelling and dynamic simulation of a parabolic trough power plant, Journal Of Process Control. 39 (2016) 123-138.

[29] W. Al-Maliki, F. Alobaid, R. Starkloff, V. Kez, B. Epple, Investigation on the dynamic behaviour of a parabolic trough power plant during strongly cloudy days, Applied Thermal Engineering. 99 (2016) 114-132.

[30] M. Proctor, W. Yu, R. Kirkpatrick, B. Young, Dynamic modelling and validation of a commercial scale geothermal organic rankine cycle power plant, Geothermics. 61 (2016) 63-74.

[31] R. Dickes, A. Desideri, I. H. Bell, V. Lemort, Dynamic modeling and control strategy analysis of a micro-scale CSP plant coupled with a thermocline system for power generation, Proceedings of Eurosun conference 2014, At Aix-les-Bains, France.

[32] P. Vitte, F. Manenti, S. Pierucci, G. Buzzi-Ferraris, Dynamic simulation of Concentrating Solar Plants, Proceedings of CHISA conference, 2012.

[33] F. Manenti, Z. Ravaghi-Ardebili, Dynamic simulation of concentrating solar power plant and two-tanks direct thermal energy storage, Energy. 55 (2013) 89-97.

[34] B. Hefni, Dynamic Modeling of Concentrated Solar Power Plants with the ThermoSysPro Library (Parabolic Trough Collectors, Fresnel Reflector and Solar-Hybrid), Energy Procedia. 49 (2014) 1127-1137.

[35] S. Rodat, J. Souza, S. Thebault, V. Vuillerme, N. Dupassieux, Dynamic Simulations of Fresnel Solar Power Plants, Energy Procedia. 49 (2014) 1501-1510.

[36] B. Twomey, P. Jacobs, H. Gurgenci, Dynamic performance estimation of small-scale solar cogeneration with an organic Rankine cycle using a scroll expander, Applied Thermal Engineering. 51 (2013) 1307-1316.

[37] M. Mitterhofer, M. Orosz, Dynamic Simulation and Optimization of an Experimental Micro-CSP Power Plant, Volume 1 (2015).

[38] C. Zhou, E. Doroodchi, B. Moghtaderi, An in-depth assessment of hybrid solar-geothermal power generation, Energy Conversion And Management. 74 (2013) 88-101.

[39] M. Antonelli, A. Baccioli, M. Francesconi, U. Desideri, Dynamic modelling of a low-concentration solar power plant: A control strategy to improve flexibility, Renewable Energy. 95 (2016) 574-585.

[40] M. Antonelli, A. Baccioli, M. Francesconi, U. Desideri, L. Martorano, Electrical production of a small size Concentrated Solar Power plant with compound parabolic collectors, Renewable Energy. 83 (2015) 1110-1118.

[41] M. Montes, A. Abánades, J. Martínez-Val, M. Valdés, Solar multiple optimization for a solar-only thermal power plant, using oil as heat transfer fluid in the parabolic trough collectors, Solar Energy. 83 (2009) 2165-2176.

[42] A. Delgado-Torres, L. García-Rodríguez, Preliminary assessment of solar organic Rankine cycles for driving a desalination system, Desalination. 216 (2007) 252-275

[43] S. Quoilin, M. Broek, S. Declaye, P. Dewallef, V. Lemort, Techno-economic survey of Organic Rankine Cycle (ORC) systems, Renewable And Sustainable Energy Reviews. 22 (2013) 168-186.

[44] AMESim User's Guide.

[45] UNI EN ISO 15927-4.

[46] M. Francesconi, Analysis and design of devices for medium temperature solar thermal energy conversion, (2017) Università di Pisa, Ph.D. Thesis. https://doi.org/10.13131/UNIPI/ETD/01092017-161721